Crystalline Colloidal Bragg Diffraction Devices: the Basis for a New Generation of Raman Instrumentation

Sanford A. Asher and Perry L. Flaugh University of Pittsburgh

Guy Washinger EG&G Princeton Applied Research

A novel optical dispersing element composed of a three-dimensionally ordered array of polystyrene spheres has been developed. This colloidal dispersion is stabilized by Coulombic repulsive interactions between spheres; each sphere has covalently attached functional groups that ionize in solution to give each sphere a net negative charge. The array forms in a hexagonal close-packed crystal structure, which is oriented between transparent plates. The lattice parameters are comparable in length to the wavelength of visible light. Thus, strong Bragg diffraction occurs from the lattice planes. This Bragg diffraction is used to prepare an optical filter that diffracts light over a small wavelength interval but lets adjacent wavelengths freely transmit. This filter is used as a Rayleigh-line rejection filter in a new Raman spectrometer, which has dramatically improved performance. This article will also discuss a number of important applications using this spectrometer.

Optical spectroscopy has played a pivotal role in the evolution of science and technology. Early spectroscopic studies of the response of materials to radiation motivated the development of quantum mechanics, the current framework used to examine theoretically molecular structure and properties. Spectroscopy is the primary experimental technique used for characterization of molecular structure. It also is the primary technique for making quantitative and qualitative analytical measurements of chemical species in the simplest, as well as the most complex, matrices. The list of different optical spectroscopic techniques is rather vast (1). A partial list, however, would include absorption spectroscopy, fluorescence spectroscopy, Raman spectroscopy, all of the elastic and quasi-elastic light-scattering techniques, linear dichroism, circular dichroism, magnetic circular dichroism, photoacoustic spectroscopy, and coherent optical phenomena such as CARS (coherent anti-Stokes Raman spectroscopy), Raman gain, and various multiphoton spectroscopies such as resonance ionization spectroscopy.

This list is ordered somewhat chronologically, and the newer coherent and multiphoton spectroscopic techniques owe their existence to the development of the laser. The routine spectroscopies, such as absorption and fluorescence, are only routine because of advances in electronic detection devices such as the photomultiplier. Indeed, the development of new devices is a major evolutionary thrust for the discovery and application of new spectroscopies, which give insight into the nature of the universe.

Raman spectroscopy has benefitted greatly from both of the above mentioned technological advances (2). Prior to the advent of the laser and the photomultiplier, Raman spectroscopy was difficult to perform and had few practitioners. The technique's major utility was for studying the vibrational structure of pure substances. The paucity of its use occurred because of the difficulty of measuring the Raman spectra; the quantum yield for Raman scattering is very small (less than 10^{-8}), the frequency shifts for vibrational Raman scattering are relatively small (about one percent of the excitation frequency in the visible spectral region), and numerous other competing optical processes, such as fluorescence, can occur to produce interfering emission.

The development of the photomultiplier began a revolution in Raman spectroscopy. The sensitivity and the large dynamic range of the photomultiplier, as well as its nearly instantaneous response (compared to the photographic plate), dramatically decreased the experimental difficulties of Raman spectroscopy. The development of commercial laser sources made Raman a straightforward technique, and commercial instruments became available. Although the activity in the field has dramatically increased during the last fifteen years, Raman has yet to become a truly routine technique. This is mainly because the nonresonance-Raman detection limit for analytes, even in pure water samples, can still be as high as 100 ppm. The recent development of optical multichannel analyzers that have greater than 10% quantum yields for photon detection has also been an important advance. The application of these devices in Raman spectroscopy has dramatically increased spectral signal-to-noise ratios and decreased detection limits by making it much easier to discriminate the sharp Raman bands from competing sample emission, which is usually broad. Researchers are now within one or two orders of magnitude of the theoretical limit for the signal-to-noise ratio possible for Raman spectral measurements. The resulting improvement in sensitivity means that Raman spectroscopy is very close to offering the sensitivity necessary for it to become a routine technique for typical dilute samples.

The next advance in Raman instrumentation must increase the spectrometer throughput as well as the spectrometer Rayleigh line rejection efficiency. Because the quasi-elastically scattered light (often misnamed the Rayleigh scattering) is so much more intense than the Raman-scattered light, it is essential that a Raman measurement selectively attenuate the elastically scattered light prior to the detector. The major approach has been to devise complex multielement spectrometers that reject the excitation wavelength but pass the spectrally

shifted Raman-scattered light. Typical stray light specifications of commercial double spectrometers are quoted as 10^{-12} at 10 band-pass units away from the Rayleigh line. These spectrometers, while partially successful, dramatically sacrifice throughput. A typical new double monochromator — used with a photomultiplier, ruled gratings at their blaze wavelength, and an exit slit — has a throughput of less than 10%. The throughput is even less for spectrometers used with multichannel detectors, because no limiting aperture (such as the exit slit) exists to prevent elastically scattered light and spectrometer stray light from hitting the photoactive portion of the detector. Because of the electronic and optical cross talk between pixels of the present generation of intensified Reticon optical multichannel detectors, the Rayleigh-scattered light must be prevented from hitting the photoactive portion of the spectrograph image plane. This restriction increases the complexity of any spectrometer designed for multichannel detection as well as decreasing its ultimate throughput.

The next obvious advance will be to improve the spectrometers and spectrographs used in Raman spectroscopy. What is required is a new optical dispersing element that selectively rejects the narrow wavelength interval of the laser excitation line would be useful. We have developed an optical dispersing device that is expected to have numerous applications in spectroscopy (3–5). This article describes the principles governing the functioning of the device and its applicability to Raman spectroscopy. This article also shows that the filter can be used to construct a new generation of Raman instrumentation.

CRYSTALLINE COLLOIDAL BRAGG DIFFRACTION FILTER

The new optical dispersing device is composed of a monodisperse colloid of polystyrene spheres. The spheres, which are approximately 100 nm in diameter, are prepared by emulsion polymerization and are synthesized with thousands of sulfate functional groups that are covalently attached to the surface of each sphere. These spheres are dispersed at an appropriate concentration in water. In solution, the protonated sulfate groups ionize (Figure 1a) to yield spheres with a net negative charge; the proton counterions are hydrated by the solution and are mobile. As is evident from electrostatics, these spheres will repel one another if they are localized within a distance that is comparable to a Debye layer thickness (6). The Debye layer represents a thickness over which the electric field due to the charge on a sphere drops to $1/e$ of its value at the surface. If the ionic strength of the solution is low, then the Debye length will be many times a sphere diameter and the repulsion between spheres will be significant over long distances.

The repulsion between the colloidal spheres is comparable to the

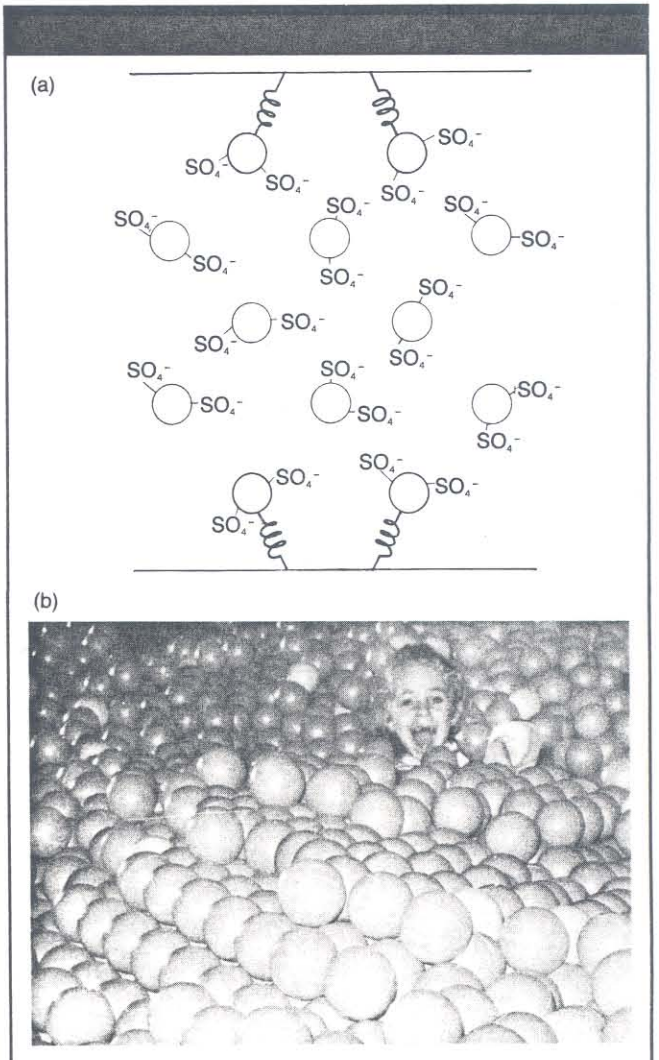

Figure 1. (a) Repulsive interactions between ionized colloidal particles. (b) Packing of plastic spheres in children's pool at Expo '86 World's Fair. (The Maxwell's Demon who is adding dynamics and novel defect structures to the array is Rachel Asher.)

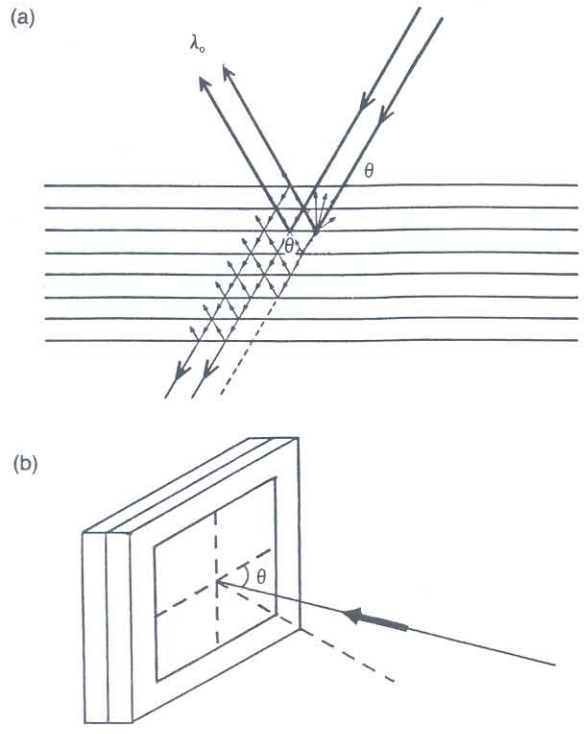

Figure 2. (a) Schematic representation of a set of layers in the colloidal crystal and the locus of incident Bragg glancing angles that fulfill the Bragg condition. (b) The orientation of a filter to the incident light beam.

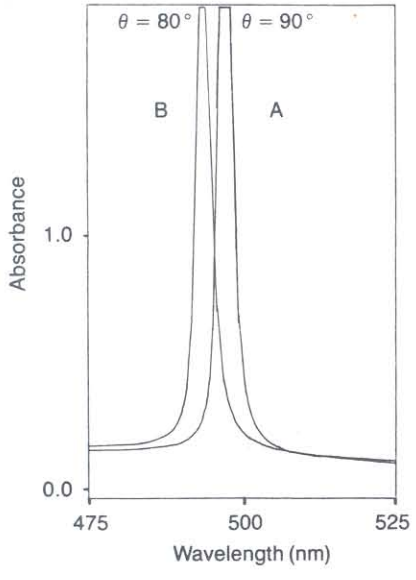

Figure 3. Spectra showing transmission through the Bragg diffraction filter as a function of filter orientation to the incident beam. At 90° incidence, the center rejection wavelength is 497 nm (A). If the filter is tilted to 80°, the rejected band shifts to 493 nm (B).

repulsion between packed hard spheres, with the exception that the colloidal spheres are soft and spongy, and forces can exist between other polystyrene spheres than just those that are nearest neighbors. The sphere packing that will occur is similar to that observed from the packing of hard spheres; Figure 1b shows the packing of plastic spheres. The spheres organize themselves into a close-packed array, developing a series of layers that are similar to lattice layers in an atomic crystal.

The spheres in the colloidal array are also close packed, but in contrast to the hard spheres, interactions between second and third nearest neighbors result in the colloidal spheres adopting a regular crystal structure that may be either face-centered cubic (FCC) or hexagonal close packed (HCP). The choice of crystal structure (which can include other types in addition to FCC and HCP) depends on such details as concentration, charge, and solution ionic strength. For the colloid discussed in this article, however, the crystal structure was determined to be HCP.

In atomic or molecular crystals, the lattice dimensions are defined by the interplay between attractive and repulsive interactions between atoms or molecules. For the colloidal system, the only important interactions between spheres are repulsive. Because the spheres cannot leave the solution, the lattice constant is completely determined by the concentration of spheres in the solution. If the sphere density is from 10^{13} to 10^{14} spheres/cm^3 the lattice parameter is comparable to the wavelength of light in the visible spectral region. This crystal structure will Bragg diffract visible-wavelength radiation in the same way that atomic crystals Bragg diffract x-ray radiation.

Filters composed of this colloid were prepared by orienting the (001) planes parallel to the plane of a pair of quartz plates enclosing the colloid. Thus, the furthest spaced set of planes are oriented with their normal perpendicular to the quartz plates. According to Bragg's law, diffraction of light will occur (Figure 2) when:

$$m\lambda_0 = 2nd \sin\theta \qquad [1]$$

where

- θ = the Bragg glancing angle (the complement of the incidence angle normally defined for reflection of light from a surface)
- λ_0 = the wavelength of light in vacuum
- m = an integer that specifies the order of diffraction (for the purposes of this discussion, $m = 1$)
- d = the spacing between planes
- n = the effective refractive index of the colloidal solution.

If polychromatic collimated light is incident at an angle θ to the filter, those wavelengths that fulfill the Bragg condition will be diffracted, while other wavelengths that do not fulfill the Bragg condition will transmit completely through the filter. Because the other sets of planes in the crystal have shorter spacings and/or are oriented at large angles from the (001) plane (which is parallel to the quartz plates), a large band pass for light exists around the Bragg diffracted wavelength.

Figure 3 illustrates the transmission spectrum for light passing through a filter that has been oriented normal to the sampling beam of a spectrophotometer. Within the stray light specification of this spectrometer, no light is transmitted at 497 nm. If a laser is used to measure transmission at the band maximum, no transmission is visually observed; this indicates a transmission of less than 10^{-8}%. The full bandwidth in this case is 8 nm to the 50% transmittance points and 2 nm to the 10% transmittance points, which corresponds at this wavelength to approximately 320 and 80 cm^{-1} full bandwidths. It should be noted that the band rejection for Raman scattering on either the Stokes or the anti-Stokes side is only one-half of this value.

The band rejection wavelength can be easily varied by tilting the filter with respect to the incident beam, as indicated in Figure 3. The dependence of the rejection wavelength on the filter angle is readily calculated from equation 1, in which the incident angle, θ_1, in the colloidal medium is calculated from Snell's law for refraction:

$$\theta_1 = \cos^{-1}[(\cos\theta_0)/n] \qquad [2]$$

and

$$m\lambda_0 = 2nd \sin\theta \qquad [3]$$

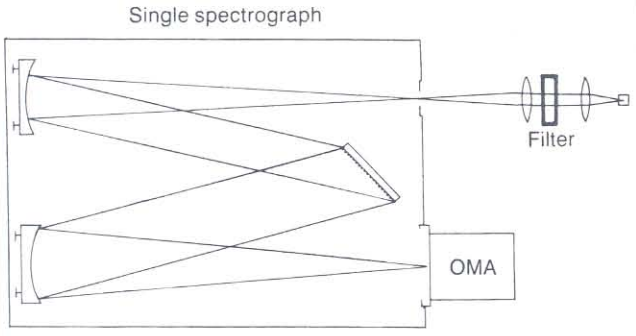

Figure 4. Block diagram of a Raman spectrometer using a crystalline colloidal Bragg diffraction filter with a 0.3-m spectrograph and an optical multichannel analyzer.

where θ is the Bragg glancing angle of incidence from the air to the filter, and the refractive index of air is taken to be one.

Recently, Spry and Kosan (7) examined the theoretical limits for the rejection efficiency and bandwidths of crystalline colloidal Bragg diffraction filters. They assumed that the sphere scattering is in the Rayleigh–Gans limit and derived relationships for both the filter transmission and its bandwidth. The filter transmission is a strong function of the relative volume of the diffractive medium occupied by the spheres. The theory permits calculation of the expected transmission by using filters of variable thickness, refractive index, incident Bragg angle, wavelength of Bragg diffraction, and sphere diameter. For example, the transmission of a 200-μm thick filter made from 91-nm spheres with an interplane spacing of 200 nm would be calculated to be less than 10^{-16}. The bandwidth can be given by the following expression, which is a simple extension of the expression formulated by Spry and Kosan:

$$\Delta\lambda = F(\theta,n,\lambda_0)\,[u^3\,2/3! - u^5\,4/5! + u^7\,6/7! - \ldots] \qquad [4]$$

where

u = $\pi\,(3/2)^{1/2} D_0/D$
D_0 = the sphere diameter
D = the next nearest neighbor spacing.

$F(\theta,n,\lambda_0)$ is a complex function of the incident angle, the refractive index of the medium, and the wavelength of diffraction. For a 500-nm diffracted wavelength, for $\theta = 90°$, and using approximately 100-nm spheres, bandwidths of about 5 nm are measured. The expression above indicates that the bandwidth should dramatically decrease with smaller sphere sizes because of the cubic and higher power dependence of bandwidth on the sphere diameter. We have experimentally demonstrated the dependence of the bandwidth on sphere diameter.

The major point is that these filters have extraordinarily high attenuation, have either large or small rejection bandwidths, and freely transmit light at wavelengths that do not meet the Bragg diffraction condition. The bandwidths of the filters are determined by the sphere size used. The bandwidth and rejection efficiencies of the filters are expected to deviate somewhat from the theoretical prediction because of factors such as mosaicity in crystal structure and orientation. Other factors that will decrease filter performance include defects, deviations in sphere position due to the thermal ellipsoid associated with sphere position, and the fact that the spheres are not completely monodisperse. In spite of these factors, the behavior of the filters is found to agree at least semiquantitatively with theoretical predictions. These crystalline colloidal Bragg diffraction filters are directly usable as prefilters to reject elastic scattering in Raman spectral measurements.

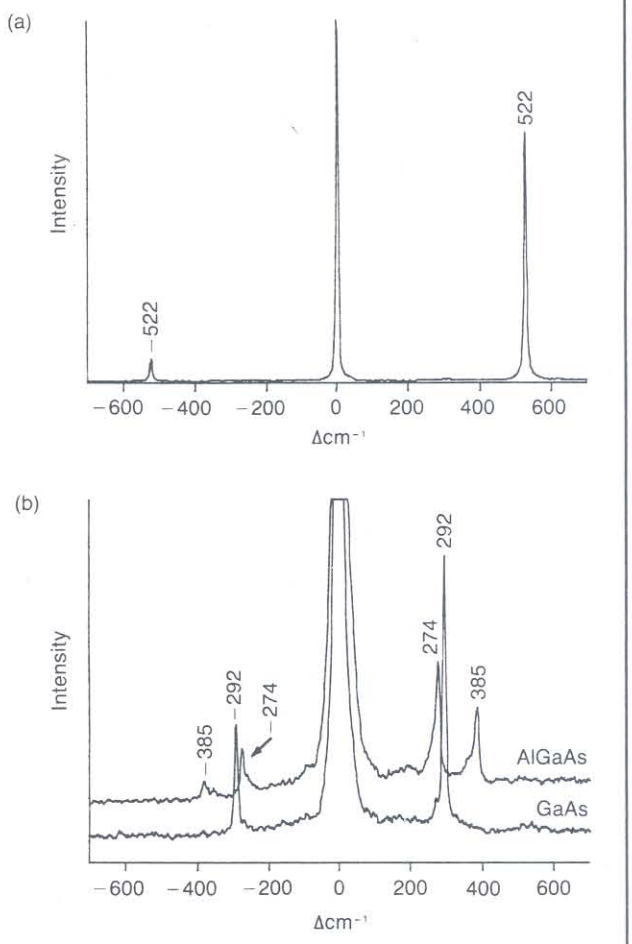

Figure 5. (a) Simultaneously measured Stokes and anti-Stokes Raman spectrum of crystalline silicon; (b) Raman spectral comparison between gallium arsenide and aluminum gallium arsenide. (The spectra were taken with the instrument diagrammed in Figure 4.)

APPLICATIONS

It is relatively simple to construct a Raman instrument based on this crystalline colloidal Bragg diffraction filter*. For example, Figure 4 shows a block diagram of a Raman spectrometer that uses the filter to reject Rayleigh-scattered light prior to the entrance slit of a 0.3-m spectrograph. The laser excitation is focused onto a sample, and the scattered light is collected and collimated by a camera lens. This collimated light is sent through the filter to reject the Rayleigh scattering. The collimated, filtered light is focused by a lens onto the slit of a simple commercial spectrograph, which in this case was a Jobin–Yvon model HR 320 (Instruments SA, Metuchen, New Jersey) with a 1200-groove/mm holographic grating. The dispersed Raman-scattered light was focused onto a EG&G Princeton Applied Research (Princeton, New Jersey) model 1421 intensified Reticon detector.

A few examples of the Raman spectra obtainable with this instrument are shown in Figures 5–7. Figure 5a shows both the Stokes and the anti-Stokes side of the Raman spectrum of crystalline silicon, which was obtained with less than 100 mW of cw argon laser excitation at 514.5 nm. This spectrum, obtained in less than 30 s, illustrates the high signal-to-noise and the excellent rejection of the Rayleigh-scattered light; the

*A prototype of this new generation instrument was displayed at the Tenth International Conference on Raman Spectroscopy in Eugene, Oregon, during September of this year.

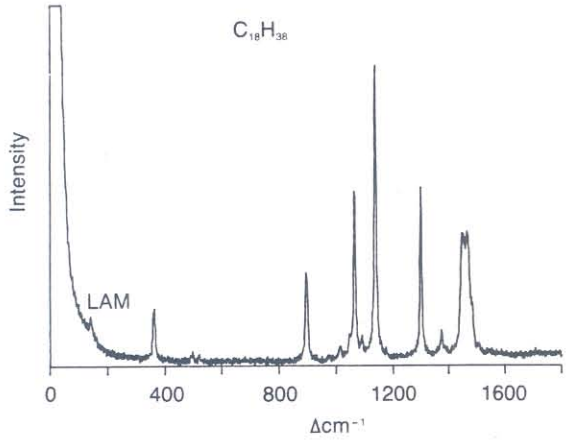

Figure 6. Raman spectrum of a saturated $C_{18}H_{38}$ hydrocarbon taken with the instrument shown in Figure 4.

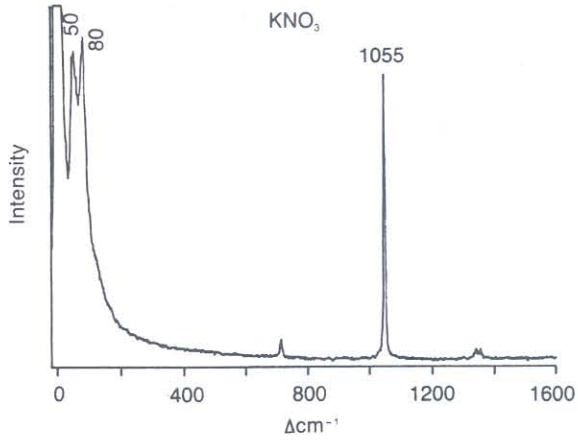

Figure 7. Raman spectrum of crystals of KNO_3 in a melting-point capillary tube taken with the instrument diagrammed in Figure 4.

Rayleigh intensity is comparable to that of the Raman intensity. The 522-cm^{-1} peaks are derived from the degenerate longitudinal and transverse optical phonons of crystalline silicon (8,9).

Figure 5b compares the Stokes and the anti-Stokes Raman spectra of gallium arsenide and gallium aluminum arsenide. The 292-cm^{-1} peak of the gallium arsenide is assigned as a longitudinal optical phonon (9). As the aluminum composition increases, characteristic spectral changes occur with a shift of the 292-cm^{-1} mode to 274 cm^{-1} and the appearance of a mode associated with an Al-As vibration at 385 cm^{-1}; this sample has the composition $Al_{0.4}$ $Ga_{0.6}$ As. The frequency of the 385-cm^{-1} band, which is also assigned to a longitudinal optical phonon, serves as a diagnostic indicator of the Al composition in this semiconductor. Raman measurements of these phonon frequencies are important in the semiconductor industry, because the data could be used to monitor the growth of layers in superlattice semiconductor materials.

A more challenging measurement is shown in Figure 6, which is a spectrum of a solid microcrystalline sample of a $C_{18}H_{38}$ saturated hydrocarbon. This sample, although highly scattering, shows high signal-to-noise even at low frequencies. Even the ~130-cm^{-1} longitudinal acoustic mode (LAM) is evident, as are the higher frequency modes associated with carbon-carbon stretching and bending and carbon-hydrogen bending. The frequency of the LAM is diagnostic of the hydrocarbon chain length and the average all-trans carbon chain length in this sample; as a result, the measured Raman spectrum, which was obtained in 10 min with 20 mW of 514.5-nm excitation, yields molecular information about macroscopic material properties.

Figure 7, which shows the Raman spectrum of crystalline KNO_3 in a capillary tube, illustrates the low-frequency performance of this spectrograph. The low-frequency doublet between 50 and 100 cm^{-1} is easily resolved, as are the higher frequency peaks. Figure 8 is a photograph of the Raman instrument built for these studies and indicates the optical simplicity of the instrumentation. The collection optics include two camera lenses and the crystalline colloidal filter.

The major limitation in rejecting the Rayleigh scattering stems from the collimation requirement; all rays at the Rayleigh wavelength must meet the Bragg-diffraction condition. This establishes criteria for the collection optics as well as for the spectrograph. Figure 9 shows an optical diagram of a novel slitless Raman instrument

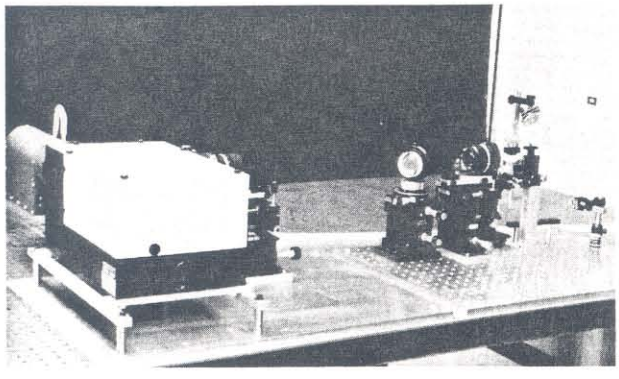

Figure 8. Photograph of the Raman spectrometer used to obtain spectra shown in Figures 5–7.

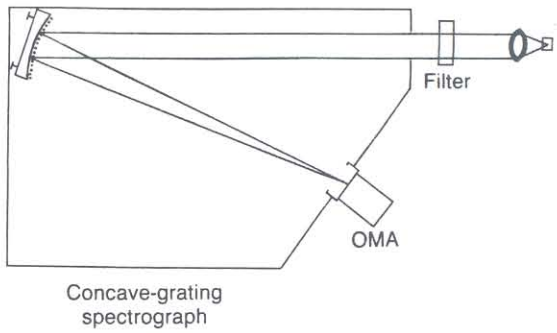

Figure 9. Block diagram of new slitless single-element high-throughput Raman spectrometer.

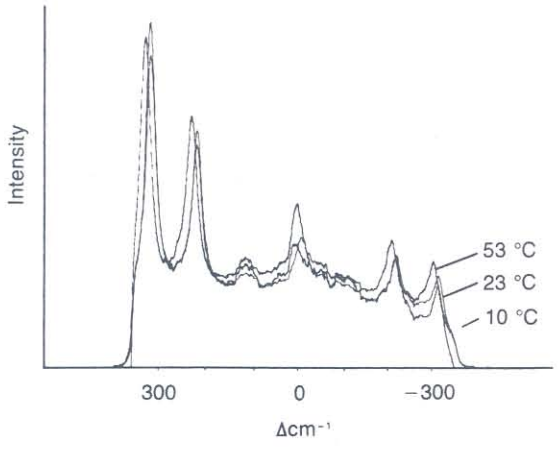

Figure 10. Simultaneously measured Stokes and anti-Stokes Raman spectra of CCl_4 measured at different temperatures. Spectra were obtained using the slitless spectrometer shown in Figure 9. Note the lack of intensity at the elastically scattered frequency (0 cm^{-1}).

that has been maximized for throughput; it contains the absolute minimum of optical components. The light scattered from a sample is collimated by a camera lens, and the light then passes through the colloidal filter. This filtered, collimated light passes through an opening that is the same size as the collimated beam (~1.5 in. in diameter) onto a concave holographic grating, which disperses and focuses the light onto the photoactive surface of the intensified Reticon detector. The resolution element for this spectrometer is defined by the width of the laser beam in the sample. Because the laser beam can be easily focused to 10 μm in transparent samples and the magnification of the system is less than 10, the linear resolution is defined by the Reticon pixel element spacing and the crosstalk between pixel elements; the frequency resolution is defined by the spectrograph dispersion.

Figure 10 shows simultaneously measured Stokes and anti-Stokes Raman spectra of CCl_4 that were obtained at different temperatures. These spectra were each measured in 0.5 s using less than 100 mW of laser power. The Rayleigh rejection efficiency of the filter is sufficient to attenuate the elastically scattered light intensity to a level less than that of the Raman scattering. It should be pointed out that nothing fancy was done with the sample solution. It was neither filtered nor distilled before use. The spectra show the temperature dependence of the Stokes/anti-Stokes intensity ratios and illustrate the increased anti-Stokes scattering as the temperature increases. In the temperature range shown here (10°–50 °C), less than a 20% change will occur in the relative integrated intensity, with the Stokes side intensity decreasing by ~8% and the anti-Stokes side increasing by a comparable amount. This behavior is clearly evident from the spectra. Obviously, this is a demonstration of one of the more expensive thermometers known, but one which could be useful for monitoring temperatures in remote hostile environments.

CONCLUSIONS

We have developed an optical dispersing element that is suitable for numerous important applications in spectroscopy and the optical sciences. One important application is in Raman spectroscopy: This filter will motivate a new generation of Raman spectrometers with improved performance. The experimental sensitivity, the signal-to-noise ratios, and the detection limits of these new instruments closely approach the theoretical limit. The resulting simplification of the instrumentation, the decreased cost, and the increased sensitivity should play a pivotal role in making Raman spectroscopy one of the routine optical spectroscopic techniques.

ACKNOWLEDGMENTS

The authors gratefully acknowledge support for this work from EG&G Princeton Applied Research and the University of Pittsburgh, and sponsorship by the Commonwealth of Pennsylvania acting through the Board of the Ben Franklin Partnership Fund, the MPC Corporation, and the Western Pennsylvania Advance Technology Center.

REFERENCES

(1) W. Demptroder, *Laser Spectroscopy: Basic Concepts and Instrumentation* (Springer-Verlag, New York, 1982).
(2) D.A. Long, *Raman Spectroscopy* (McGraw-Hill, New York, 1977).
(3) R.J. Carlson and S.A. Asher, *Appl. Spectrosc.* **38,** 297 (1984).
(4) P.L. Flaugh, S.E. O'Donnell, and S.A. Asher, *Appl. Spectrosc.* **38,** 847 (1984).
(5) S.A. Asher, U.S. and foreign patents pending.
(6) R.J. Hunter, *Comprehensive Treatise of Electrochemistry I,* J.O'M. Bockris, B.E. Conway, and E. Yeager, eds. (Plenum Press, New York, 1980), p. 397.
(7) R.J. Spry and D.J. Kosan, *Appl. Spectrosc.* **38,** 782 (1986).
(8) F.H. Pollak, *Microscience* **6,** 185 (1984).
(9) R. Tsu, *Proc. Soc. Photoopt. Instr. Eng.* **276,** 78 (1981).

***Sanford A. Asher** is associate professor in the department of chemistry, University of Pittsburgh, Pittsburgh, Pennsylvania 15260. Asher is an established investigator of the American Heart Association. He received his PhD in chemistry in 1976 from the University of California, Berkeley, working in the laboratory of Ken Sauer and was a postdoctoral fellow in applied physics at Harvard University with Peter Pershan. Asher received his BA in 1971 from the University of Missouri, St. Louis.*

***Perry L. Flaugh** is a graduate student in the chemistry department at University of Pittsburgh. He received his B.S. at Juniata College.*

***Guy Washinger** is marketing manager, spectroscopy systems, at EG&G Princeton Applied Research, Scientific Instruments Division, P.O. Box 2565, Princeton, New Jersey 08543-2565.*■■